REVIEW

Check for updates

Versatile construction of a hierarchical porous electrode and its application in electrochemical hydrogen production: a mini review

Zizai Ma,[ab] Hefeng Yuan,[b] Jiaqi Sun,[b] Jie Yang,[b] Bin Tang,[b] Xiaoguang Wang [ID] *[ab] and Jinping Li [ID] *[a]

The rational design of earth-abundant transition metal-based porous electrodes is of great importance for developing next-generation electrocatalysts for water splitting. Solid–vapor treatment is a simple and versatile synthetic method to prepare transition metal compound related architectures. With this great synthetic methodology, transition metal-based hierarchical porous electrodes with well-controlled composition and geometrical configuration have been rationally fabricated. The reaction mechanism of solid–vapor methodology in preparing transition metal based hierarchical porous catalysts and recent advances for electrochemical water splitting are illustrated and discussed. The current challenges and future prospects are also provided to stimulate the development of promising transition metal-based hierarchical porous electrodes for commercial applications.

Introduction

Energy is an important material foundation for the development of human society. The large-scale exploitation and utilization of traditional fossil energy with limited reserves has led to severe environmental challenges, such as harmful pollution and the greenhouse effect, which have seriously hindered the sustainable development of society.[1–3] As a clean secondary energy source, hydrogen has been considered as an ideal energy carrier with high mass–energy ratio, and its combustion products are non-polluting. A variety of strategies have been adopted to produce hydrogen, among which electrochemical water splitting has been regarded as one of the most promising routes.[4–6] Water splitting consists of two half reactions, hydrogen evolution reaction (HER) and oxygen evolution reaction (OER), and it requires highly active electrocatalysts to overcome the sluggish reaction kinetics and improve the reaction rates at low overpotentials.[7,8] Therefore, developing suitable catalysts is of great importance for efficient electrochemical water splitting. Precious metals and their oxides such as Pt, Pd, RuO_2, *etc.* have been proved as superior catalysts for water splitting.[9,10] However, the scarcity and high price considerably limit their large-scale application. Fortunately, transition metals such as Ni, Co,

Fe, and Mo and their sulfides, phosphides, borides, selenides and tellurides have been proven as promising alternatives to replace precious metal catalysts, and these catalysts have been reported with outstanding HER or OER activities and excellent stability.[11–14] Moreover, some of these show bifunctional properties, which greatly simplifies the design process of the catalysts and pushes its potential for practical application.[15,16]

Within the various catalyst synthetic processes, solid–vapor methodology attracts widespread attention from researchers due to its versatility, accessibility and variety.[17–19] Great progress has been made in transition metal-based hierarchical porous catalysts *via* this strategy.[20–22] On the one hand, from the viewpoint of nanostructure engineering, porous nanostructures with numerous dimensions have been successfully fabricated, such as nanoparticles, nanowires, nanosheets, nanopolyhedra and so on.[23–25] And these porous architectures provide large internal reactive surface areas, straightforward mass and electron transport through a broad "highway" for electrochemical reactions.[26,27] On the other hand, from the perspective of ingredients, transition metal-based sulfides, phosphides, borides, selenides, tellurides and other derivatives as efficient catalysts have been broadly reported.[28–31] The coupling of several metallic or nonmetallic elements provides a favorable approach for the development of efficient and practical catalysts.[32–34]

In this review, we are trying to provide an understanding of recent advances in solid–vapor methodology as a versatile strategy to construct catalysts for water splitting. We have summarized the fabrication process and mechanism, and the microstructure of transition metal-based hierarchical porous

[a] Shanxi Key Laboratory of Gas Energy Efficient and Clean Utilization, Taiyuan, Shanxi, 030024, P. R. China. E-mail: jpli211@hotmail.com

[b] Laboratory of Advanced Materials and Energy Electrochemistry, Institute of New Carbon Materials, Taiyuan University of Technology, Taiyuan, 030600, P. R. China. E-mail: wangxiaoguang@tyut.edu.cn

electrodes and their electrochemical applications. In each section, representative and well-recognized works will be discussed thoroughly, with a focus on characterization and catalytic mechanism proposals. Finally, the challenges and future opportunities in developing efficient catalysts for water splitting through solid–vapor methodology are stressed.

Preparation and reaction mechanism of transition metal-based hierarchical porous electrodes

Solid–vapor treatment (Fig. 1) has been widely used to produce several transition metal-based catalysts, including transition metal sulfides, phosphides, borides, selenides, tellurides and other derivatives.[35–37] Generally, it is conducted by high temperature reactions under protective gas flow by putting a non-metallic source on the upstream and the metal precursors on the downstream in the furnace tube. In the process, the powder on the upstream converts to vapor-phase at high temperature and reacts with the precursor material as the gas flow passes to the downstream. Typically, non-metallic sources mainly include the simplest raw materials such as red phosphorus, sodium hypophosphite, sulfur powder, boron powder, selenium powder, tellurium powder, *etc.* On the other hand, the transition metal precursor is usually a transition metal foam/metal foil, or metal oxide/hydroxide supported on substrates such as carbon cloth and carbon paper.[38–40] In terms of element composition, the essence of the solid–vapor method is that the gas phase (Se, P, S, Te, *etc.* gas or related elemental compounds) reacts with the precursor (single metal, alloy or compound) at high temperature to generate ionic compounds. The anion and cation of the final product depend on the solid precursor (determining the cation) and gas phase (determining the anion), respectively. According to the principle of crystal growth kinetics, nanocrystalline grains will grow along the growth direction with the lowest energy, that is, the preferred orientation. Thus, some of the formed structures are nanowires, while some are nanosheets or other topography by the solid–vapor method.[41,42] Meanwhile, the growth environment also plays a key role in the formation of different nanostructures. The reaction temperature, pressure, time, concentration, *etc.* are all influential factors. In other words, the different topography structure depends not only on growth kinetics, but also on thermodynamics.

This method realizes the extensive growth of transition metal-based porous nanostructures in large scale and with high quality on different substrates for hydrogen or oxygen evolution. Firstly, the preparation of the catalyst and that of the electrode are integrated, which shortens the fabrication process
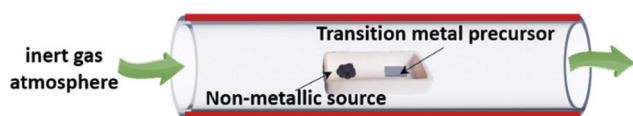
and reduces the cost. Moreover, binding agents are no more required because of the superior interfaces between nano-catalysts and substrates, thus reducing the contact resistance and facilitating charge transportation. What's more, the component of products could be easily regulated to improve the physical and chemical properties by tailoring the ratio of precursors and fabrication parameters. With these benefits, many projects have been proposed to enhance the catalytic activity of transition metal-based catalysts for water splitting *via* solid–vapor routes.[43,44]

Nanostructures of transition metal-based hierarchical porous electrodes *via* solid–vapor treatment

Nanostructure is one of the key factors in improving the efficiency of electrodes for water splitting. Specifically, nano-structures with various dimensions and morphologies have been explored by solid-vapor treatment. In this section, we will summarize the recent advances in nanostructure engineering of transition metal-based catalysts through this strategy.

Nanoparticles

Sung and co-workers[45] reported a simple and effective approach to prepare high-performance iron phosphide (FeP) nanoparticle electrocatalysts (Fig. 2). In the preparation, polydopamine-coated iron oxide nanoparticles are thermally treated with a phosphorus source. Through a single-step heating procedure, carbonization of the dopamine coating and phosphidation of iron oxide nano-particles take place simultaneously, producing carbon-shell-coated FeP nanoparticles. And nanoparticles with different sizes can be prepared by tuning the heat treatment procedures. Furthermore, they demonstrated that carbon-shell-protected FeP nanoparticles have both high catalytic activity and long-term durability for HER.
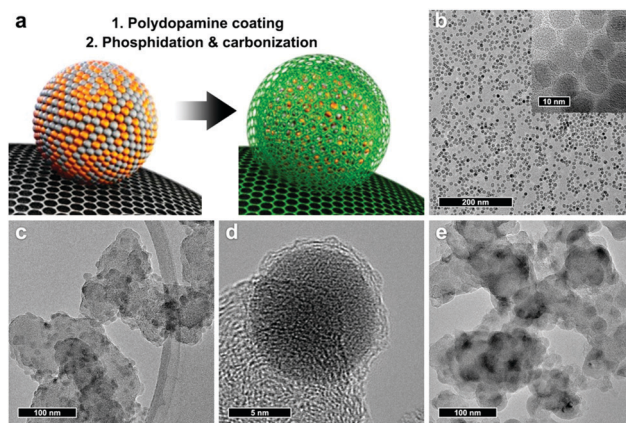

Fig. 2 (a) Schematic representation of carbon-shell-coated FeP NP preparation. (b–e) TEM images of as-synthesized iron oxide NPs (b), carbon-shell-coated FeP NPs (c and d), and FeP NPs prepared without the carbon shell (e).[45] Reproduced with permission from ref. 45. Copyright 2017, American Chemical Society.

Fig. 1 A schematic of the fabrication processes of transition metal-based hierarchical porous electrodes *via* the solid–vapor method.

Solid–vapor treatment is a simple and versatile synthetic method for synthesizing catalyst materials, which not only yields the corresponding product from one kind of non-metal source and transition metal source, but also combines several metal source precursors and non-metal sources to prepare hybrids or compounds.[46–48] For example, Yu et al.[49] proposed small $FePSe_3$ nanoparticles anchored on a N-doped carbon framework ($FePSe_3$/NC) synthesized by high-temperature carbonization, followed by simultaneous phosphorization and selenization. The resulting highly open carbon framework contributed to large surface area of host $FePSe_3$ nanoparticles. The small nanoparticles with a metallic nature and high electrical conductivity can expose more accessible edge sites, producing a moderate hydrogen adsorption Gibbs free energy. As a result, the as-synthesized $FePSe_3$/NC exhibited remarkable HER catalytic activity in a wide pH range, belonging to the advanced non-noble-metal electrocatalyst. An FeP/Ni_2P hybrid nanoparticle catalyst[50] supported on 3D Ni foam was prepared by twice phosphidation of a bimetallic precursor, which exhibited both extremely high OER and HER activities in the same alkaline electrolyte. This work proves once again the flexibility and universality of the solid–vapor methodology.

Nanowires

The nanowire structure is another popular and attractive morphology for designing highly efficient electrocatalysts.

Sun's group have reported a series of phosphide nanowire catalysts by solid–vapor treatment, such as FeP,[51] CoP,[52] Al-doped CoP,[53] Cu_3P,[54] etc. Li et al. decorated CoP hybrid nanowires with PANI nanodots, which would favor proton acceptor ability and accelerated electron transfer for HER.[55]

Additionally, as shown in Fig. 3, N doped 3D dandelion-flower-like CoS_2 nanowires with many branched needles on Ni foam (N-CoS_2/NF) were developed by using NH_4HCO_3 and sulfur powder as N and S sources, respectively.[56] The TEM image showed porous structures in the nanowire arrays. Numerous lattice defects (marked by a circle) suggested more active sites, which was conducive to the enhanced electro-catalytic activity. Co, S and N elements were distributed homogeneously on the nanorods, indicating the successful N doping. Owing to the fact that more electrons around Co atoms will transfer to N atoms than to S atoms, the positively charged Co-top sites and Co-bridge sites were beneficial for H_2O adsorption and H* adsorption, respectively. So, the resulting N-CoS_2/NF acting as both anode and cathode exhibited an outstanding electrocatalytic performance for overall water splitting in alkaline media.

Kuang et al. fabricated a bimetallic sulfide hybrid nanowire (NiS_2/MoS_2 HNW), which showed an efficient HER activity over a wide pH range.[57] After S vapor deposition, the NiS_2/MoS_2 HNW had a rougher surface, composed of highly dispersed 2D MoS_2 nanoplates and nanosized NiS_2 particles in this case,
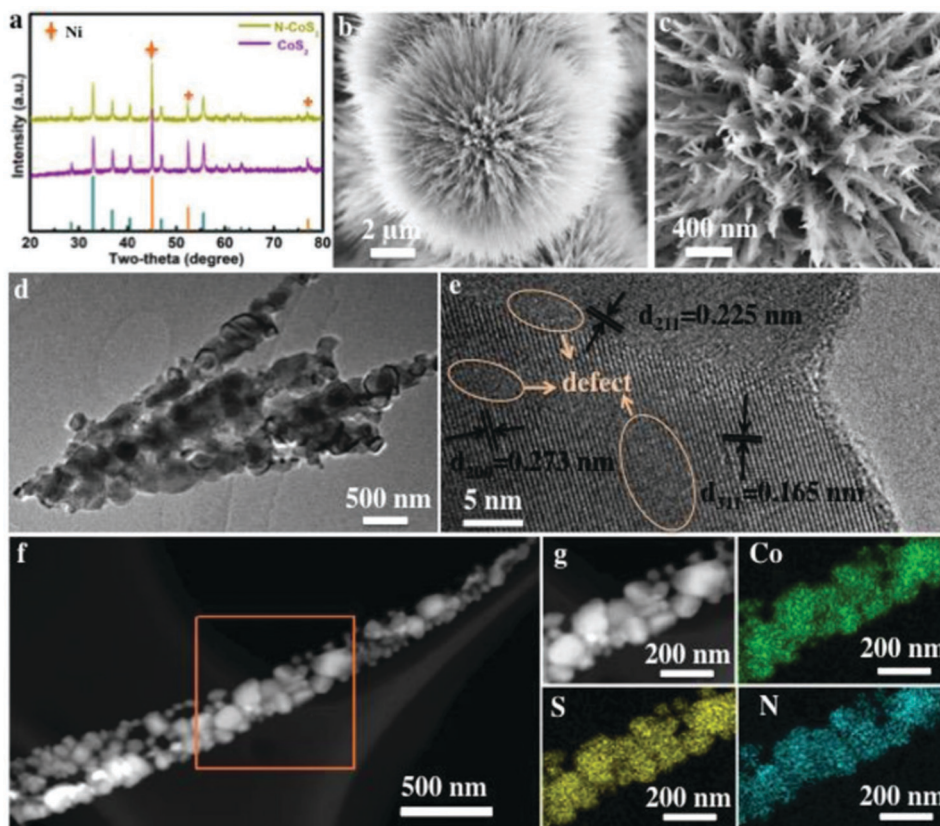

Fig. 3 (a) XRD pattern; (b and c) SEM image; (d) TEM image; (e) HRTEM; (f and g) HADDF–STEM image and the corresponding elements' mapping image of N-CoS_2.[56] Reproduced with permission from ref. 56. Copyright 2019, Wiley-VCH.

creating a hierarchical and porous structure. The special rough and porous 1D nanowires favored fast electron/mass transfer from the interior and surface of the catalyst. The Ni site served as an excellent OH adsorption center and the Mo site possessed superior adsorption capability for H*, lowering the energy barrier and accelerating the sluggish HER kinetics.

Our group also developed Al-doped CoS_2 nanowire catalysts by solid–vapor treatment.[58] Specifically, the rigid Al–Co (Al_9Co_2) intermetallic nanoporous framework was obtained via the selective etching of α-Al phase through dealloying of the $Al_{90}Co_{10}$ (at%) plate. After suffering a facile solid–vapor sulfurization toward the dealloying-derived Al–Co intermetallic sample, a self-supported Al-doped CoS_2 electrode (Al-CoS_2) was constructed (Fig. 4). Such hierarchical topography comprising both continuous 3D micron-level ligament-channel network and high-density hair-like nanowires on the ligament surface not only can provide more active sites for the adsorption of intermediate H* but is also good for releasing the detached bubbles during the HER process, thus effectively reducing the overpotential so as to enhance the HER performance.

Nanosheets

Sheet-like structures are the most common morphology and have been extensively studied by many researchers. The 2D lateral structure with coupled heterogeneous components along the intraplane direction rather than the vertical direction enables exposure of abundant active sites completely on the catalyst surface and increase the contact with the electrolyte. Owing to its good structural stability, large exposed surface area

and high mass loading of active species, excellent HER or OER performance can be realized by tuning microstructure size and composition.[59–61] For instance, a 2D Fe-containing cobalt phosphide/cobalt oxide (Fe-CoP/CoO) lateral heterostructure was synthesized via a selective low-temperature phosphorization process.[62] The as-prepared Fe-CoP/CoO configured with logical component design and in-plane component tunability exhibited a strong interfacial coupling effect between cobalt phosphide (CoP) and cobalt oxide (CoO). Benefited from the promising direct and full contact with the electrolyte, Fe-CoP/CoO shows superior electrocatalytic OER performance. Wang et al. reported Ni_5P_4–Ni_2P (Fig. 5)[63–65] and Ni–Fe–P[66] nanosheet arrays on Ni foam or carbon fiber paper by a convenient one-step phosphorization treatment. The 3D microporous skeleton covered with high-density upright nanosheets not only maximizes the number of exposed active sites, but also facilitates the diffusion of the electrolyte and the release of generated gas bubbles.

Similarly, many heterogeneous electrocatalysts are designed by strong coupled compounds. The 3D hierarchical architecture of Ni_2P–Ni_3S_2/NF displayed extremely high catalytic activity and outstanding stability toward both HER and OER. This was attributed to the strong coupling interactions between Ni_2P and Ni_3S_2 effectively regulating the electronic structure and decreasing the energy barrier.[16] 2D nanoheterojunctions between homologous CoP/NiCoP nanosheets on a N-doped carbon (NC) matrix were prepared via successive carbonization and phosphorization. Owing to the large surface area of C_3N_4 nanosheets, well-dispersed CoP/NiCoP nanoheterojunctions could be largely exposed to not only increase the contact area with electrolyte but also accelerate the rapid interfacial charge transfer. The resulting CoP/NiCoP/NC hybrid exhibited remarkable HER activities and excellent long-term stability over a wide pH range.[67]

Mixed-transition-metal (MTM)-based electrocatalysts generally exhibit desirable electrical conductivity and synergistic electronic modulation of multi-metal atoms. Anion regulated Ni/Co-based electrocatalysts (Ni–Co–A, A = P, Se, O) have the structural characteristic of holey nanosheets. It was discovered that P
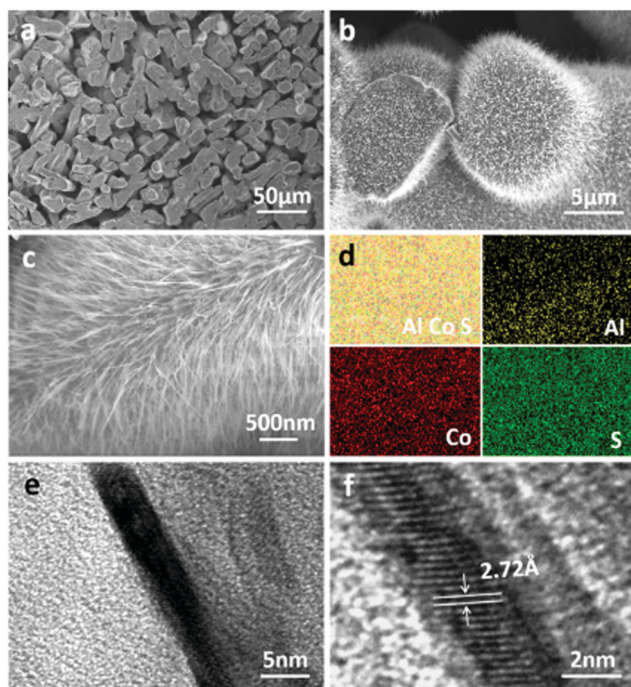

Fig. 4 (a) Low- and (b and c) high-magnification SEM images of Al-CoS_2. (d) The corresponding EDX elemental mapping of Al, Co and S. (e) TEM and (f) HRTEM images taken from a single Al-CoS_2 nanowire.[58] Reproduced with permission from ref. 58. Copyright 2019, American Chemical Society.
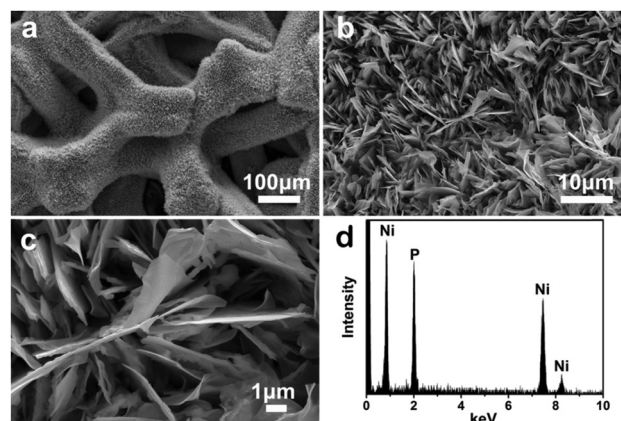

Fig. 5 (a) Low- and (b and c) high-magnification SEM images of the Ni_5P_4–Ni_2P–NS array cathode. (d) EDX spectrum.[63] Reproduced with permission from ref. 63. Copyright 2015, Wiley-VCH.

substitution could tune the electron configuration and lower the H* adsorption energy on the active sites greatly of Ni–Co–P holey nanostructures. Therefore, the NCP catalyst had an ultralow overpotential of 58 mV at 10 mA cm^{-2}.[68] Similarly, Co, Fe co-doping in NiSe$_2$ can contribute to a strong electronic interaction between the cations and significant lattice distortion, which could increase the number of active sites. The as-prepared Fe$_{0.09}$Co$_{0.13}$–NiSe$_2$ nanosheet array, based on a vapor selenization technique, was composed of densely packed nanoparticles (Fig. 6). The local wavy lattice structure was caused by the incorporation of Co and Fe into the NiSe$_2$ lattice optimizing the adsorption energy of reaction intermediates. Furthermore, this holey structure was advantageous for the penetration of the electrolyte, electron transfer and gas bubble release.[69] The as-prepared WS$_2$/CoS$_2$ heterostructure, based on the reaction of a Co–MOF precursor with Na$_2$WO$_4$ solution and then sulfurization, can provide good electrical conductivity, sufficient active sites, and modulated coordination and electronic properties, with outstanding HER activity at all pH values.[70]

Nanopolygons

Nanoframes are generally prepared by template growth, framework etching, and chemical vapor deposition. Lian *et al.*[71] adopted bimetallic MOF–Co–Fe Prussian blue analogues (Co–Fe PBAs) as the structural template, followed by etching with urea and phosphorizing with sodium hypophosphite, and fabricated nanoframes of Co–Fe phosphides as the bifunctional electrocatalyst for overall water splitting (Fig. 7). The outstanding performance is attributed to the enhanced electrochemically active surface area, and the promoted mass diffusion and charge transportation. Assembling porous and/or hollow structural framework are important prerequisites for achieving a large surface area with numerous active sites and better reaction kinetics and stability. M-doped CoP (M = Ni, Mn, Fe) hollow polyhedron frames (HPFs) were synthesized by a self-templating transformation strategy on a ZIF-67 template and subsequent oxidation and phosphidation.[72] Likewise, a tetrahedral nanocage-like NiS$_2$/NiSe$_2$ heterostructure was formed during the simultaneous sulfuration/selenylation process by using a Ni-based acetate hydroxide precursor. The porous nanopolygon morphology can expose more accessible active sites and provide a convenient charge/ionic diffusion pathway. The NiS$_2$/NiSe$_2$ heterostructure could effectively regulate the interfacial electronic structure for modulating the adsorption behavior of oxygen-containing intermediates in the OER process.[73] Similarly, Liu *et al.* developed regular hollow polyhedral cobalt phosphide (CoP hollow polyhedron) electrocatalysts for HER and OER templated by Co-centered MOFs through simple oxidation and phosphorization calcination.[74] You *et al.* prepared Co–P/NC catalysts by direct carbonization of a Co-based zeolitic imidazolate framework (ZIF-67) followed by phosphidation. Benefiting from the large specific surface area, controllable pore texture, and high nitrogen content of the ZIF (a subclass of metal–organic frameworks), the optimal Co–P/NC showed a high specific surface area of 183 m^2 g^{-1} and large mesopores, and exhibited remarkable catalytic performance for both HER and OER.[75] He *et al.* reported Fe-doped cobalt telluride nanoparticles encapsulated in nitrogen-doped carbon nanotube frameworks (Fe–Co$_{1.11}$Te$_2$@NCNTF) by tellurization of Fe-etched ZIF-67 under a mixed H$_2$/Ar atmosphere.[76]

In general, a suitable template is needed to realize porous nanopolygon morphology. Metal–organic frameworks (MOFs) are often utilized as sacrificial templates to synthesise porous and electroactive materials.[77,78] Combined with the solid–vapor method, various nanopolygon catalysts can be rationally designed for different applications.[79,80]

Electrochemical applications

Hydrogen evolution reaction

Hydrogen as a clean and renewable energy has long been expected to replace finite fossil fuels for future energy infrastructure. Electrocatalytic water splitting is an important technology for producing hydrogen in high purity and large quantities.[81,82] So far, Pt-based precious metals are still the state-of-the-art catalysts for hydrogen evolution. However, the
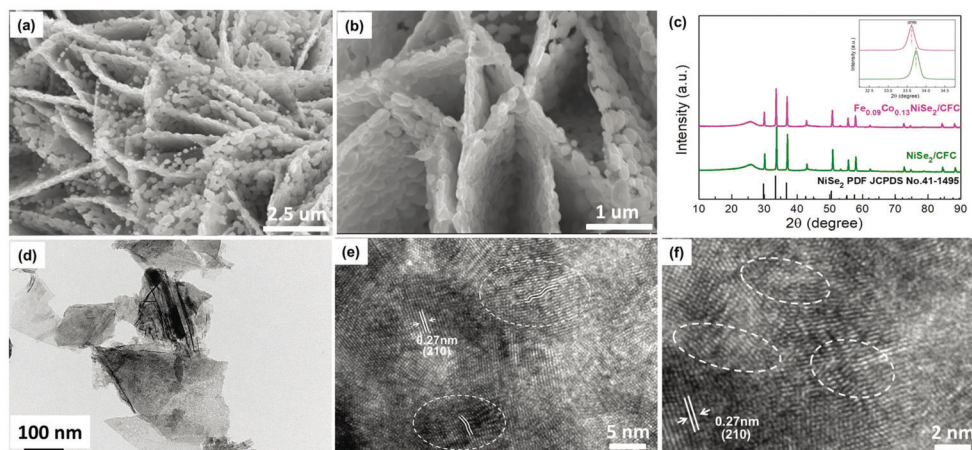

Fig. 6 Morphology and composition of the dual-cation-doped NiSe$_2$ nanosheets. (a and b) SEM images, (c) XRD pattern, (d) TEM images, and (e and f) high resolution TEM image of the Fe$_{0.09}$Co$_{0.13}$–NiSe$_2$ nanosheets.[69] Reproduced with permission from ref. 69. Copyright 2018, Wiley-VCH.
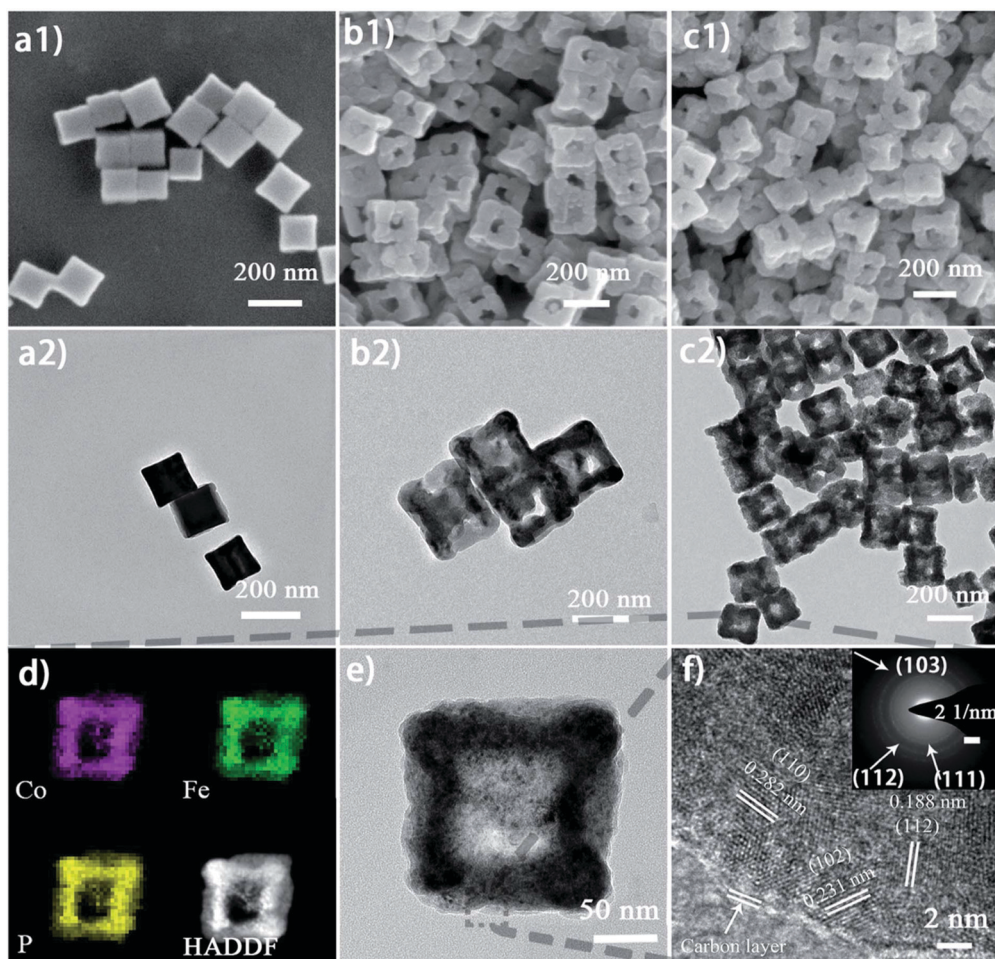
Fig. 7 (a1) and (a2) SEM and TEM images of the Co0.6Fe0.4 PBA nanocubes without etching; (b1) and (b2) SEM and TEM images of Co0.6Fe0.4–1.125 nanoframes before phosphorization; (c1 and c2) SEM and TEM images of Co0.6Fe0.4P–1.125 nanoframes after phosphorization; (d) elemental mapping images of an individual Co0.6Fe0.4P–1.125 nanoframe showing the uniformly distributed Co, Fe, and P elements; (e and f) HR-TEM and SAED images of Co0.6Fe0.4P–1.125 showing polycrystalline lattice fringes.[71] Reproduced with permission from ref. 71. Copyright 2019, Royal Society of Chemistry.

high cost and limited reserve of Pt-based electrocatalysts require seeking for highly efficient non-noble metal catalysts. Therefore, it is important to explore highly active and stable nonprecious-metal catalysts to resolve the problems of leaching or corrosion in a strong acidic or alkaline electrolyte.

Many efforts have been made to design a hybrid catalyst with different components to effectively facilitate different parts of the multistep HER process, which should consist of a water dissociation promoter for accelerating the sluggish water adsorption and dissociation dynamics.[83] The CoS|Ni|P catalyst was prepared by the following steps: electrodeposition, sulfurization, soak in Ni-ink and phosphorization.[84] As shown in Fig. 8, the as-obtained CoS|Ni|P was composed of densely packed nickel phosphide nanoparticles (NiP_2/Ni_5P_4) and cobalt phosphosulfide/phosphide ($CoPS/CoP_3$) nanosheets. CoS|Ni|P displayed outstanding electrochemical activity delivering a geometric current density of 10 mA cm^{-2} at 41 mV, comparable to that of Pt wire (31 mV) and outperforming many reported transition-metal phosphides, selenides, and sulfides. And there was no obvious decrease of the cathodic current density of the

polarization curve after 5000 CV cycles, showing its good durability. The unique hybrid structure with increased surface area and the advantages of high porosity, good electrical contact between the catalyst and the conductive support, fast charge transfer between the electrolyte and the catalyst surface are the reasons for the fast reaction kinetics for the HER process. Besides, $CoP/Ni_5P_4/CoP$,[39] CoP/CoP_2,[85] NiS_2/MoS_2,[57] $Co_9S_8@MoS_2$,[86] Ni–$MoSe_x@CoSe_2$,[87] etc. have also been proved to be efficient electrocatalysts for the HER.

Alternatively, heteroatom doping is another general pathway to improve the electrocatalytic activity by regulating the crystal structures and modulating the electronic structures. And the influence of alien-metal dopants via solid–vapor treatment on the regulation of the electronic structure of electrocatalysts has been extensively investigated. Liao et al. have developed selenium-doped MoS_2 (Se-MoS_2) particles uniformly distributed on 3D interwoven cobalt diselenide ($CoSe_2$) nanowire arrays acting as conductive scaffolds.[83] The synthesis has undergone two selenization processes, the first is to prepare $CoSe_2$, and the second step is to dope Se into MoS_2. As a result, the
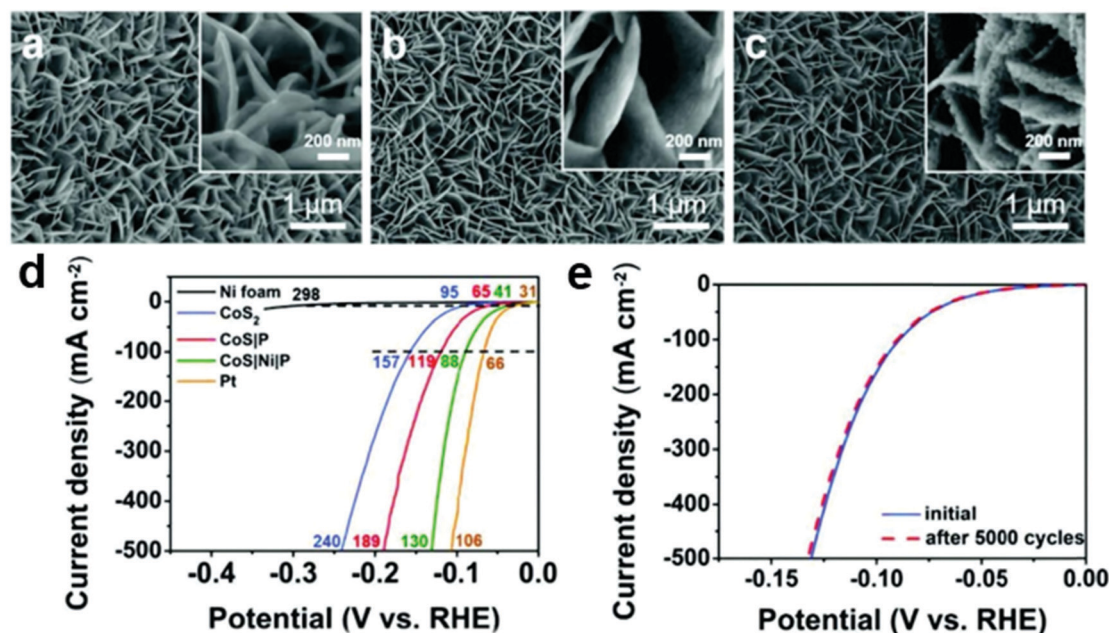
Fig. 8 Typical SEM images of (a) CoS$_2$, (b) CoS|P, and (c) CoS|Ni|P at different magnifications. (d) The polarization curves of Ni foam, CoS$_2$, CoS|P, CoS|Ni|P, and Pt wire electrodes. (e) Cycling stability of CoS|Ni|P before and after 5000 cycles.[84] Reproduced with permission from ref. 84. Copyright 2019, Wiley-VCH.

heterogeneous Se-MoS$_2$/CoSe$_2$ exhibits an outstanding catalytic HER performance with extremely low overpotentials of 30 and 93 mV at 10 and 100 mA cm^{-2} in base, respectively (Fig. 9). Moreover, this hybrid catalyst shows exceptional catalytic performance with very low overpotentials of 84 and 95 mV at 10 mA cm^{-2} in acidic and neutral electrolytes, respectively, implying robust pH universality of this hybrid catalyst. Due to the metallic nature of Se, the substitution of S by Se not only improves the electrical conductivity of 2H-MoS$_2$, but also increases the edge site density in Se-MoS$_2$ particles relative to MoS$_2$ particles, because the Gibbs free energy for hydrogen adsorption on both Se-edge and Mo-edge of MoSe2 is lower than that of the active Mo-edge in MoS$_2$. The rough and curved structures were very beneficial for exposing edge sites of layered transition metal chalcogenides.

In addition to the common Fe, Co, Ni and Mo-based transition metal catalysts, Ta, Nb, V-based catalysts can also be synthesized by the solid–vapor method.[88] Recently, vertically oriented 1T-TaS$_2$ nanosheets on nanoporous gold substrates have been reported,[89] *via* a facile solid–vapor route. They were employed to synthesize TaS$_2$ directly on the nanoporous gold substrate with sulfur and tantalum pentachloride as precursors. After 5 min growth, large-area, uniform and vertical nanosheets were observed on the NPG substrate as revealed by scanning electron microscopy (SEM) characterization (Fig. 10). By virtue of the abundant edge sites and excellent electrical transport property, such vertical 2H-TaS$_2$ nanosheets are employed as high-efficiency electrocatalysts in the hydrogen evolution reaction, featured with a rather low Tafel slope of 50 mV dec^{-1} and an overpotential (at 10 mA cm^{-2}) of 113 mV. H-TaS$_2$ flakes hybridized with TaSe$_2$ flakes were synthesized by Najafi *et al.* as heterogeneous stacking of Se- and S-based

group 5-TMDs can enhance the HER activity of S-based parts.[88] The H-TaS$_2$ flakes hybridized with the H-TaSe$_2$ flakes promoted an electron transfer from H-TaSe$_2$ flakes to H-TaS$_2$ flakes, effectively decreasing the ΔG_H of the H-TaS$_2$ basal planes toward the ideal 0 eV. The H-TaS$_2$:H-TaSe$_2$ heterogeneous catalyst outperforms its single counterparts in 0.5 M H$_2$SO$_4$ and 1 M KOH, showing an overpotential at a cathodic current density of 10 mA cm^{-2} of 120 and 230 mV respectively.

Oxygen evolution reaction

The anode reaction of water splitting, oxygen evolution reaction (OER), plays a crucial role in the green technology. However, the anode half reaction is kinetically sluggish owing to its four-electron-transfer process, which requires a large amount of energy to produce H$_2$ at a practical rate. Thus, developing high-performance OER electrocatalysts is highly desirable. At present, precious metal oxides (RuO$_2$/IrO$_2$) are still regarded as the benchmark OER electrocatalysts. Their commercial applications are severely limited by high cost and scarcity. Therefore, development of non-precious metal catalysts for OER is a key to open the door to large-scale application of hydrogen fuel. In this section, we mainly focus on some non-precious metal OER catalysts prepared by the solid–vapor method.

Transition metal borides have shown great promising OER catalytic activity, which is generally attributed to their partially amorphous structure with abundant atomic defects and the amount of undercoordinated metal atoms.[90,91] Various morphologies can be obtained through the solid-phase boronation process. For instance, 3-dimensional (3D) CoNi foam was used as a bimetal source to fabricate *in situ* ultra-thin Co–Ni–B nanoflakes by reacting with amorphous boron powder at
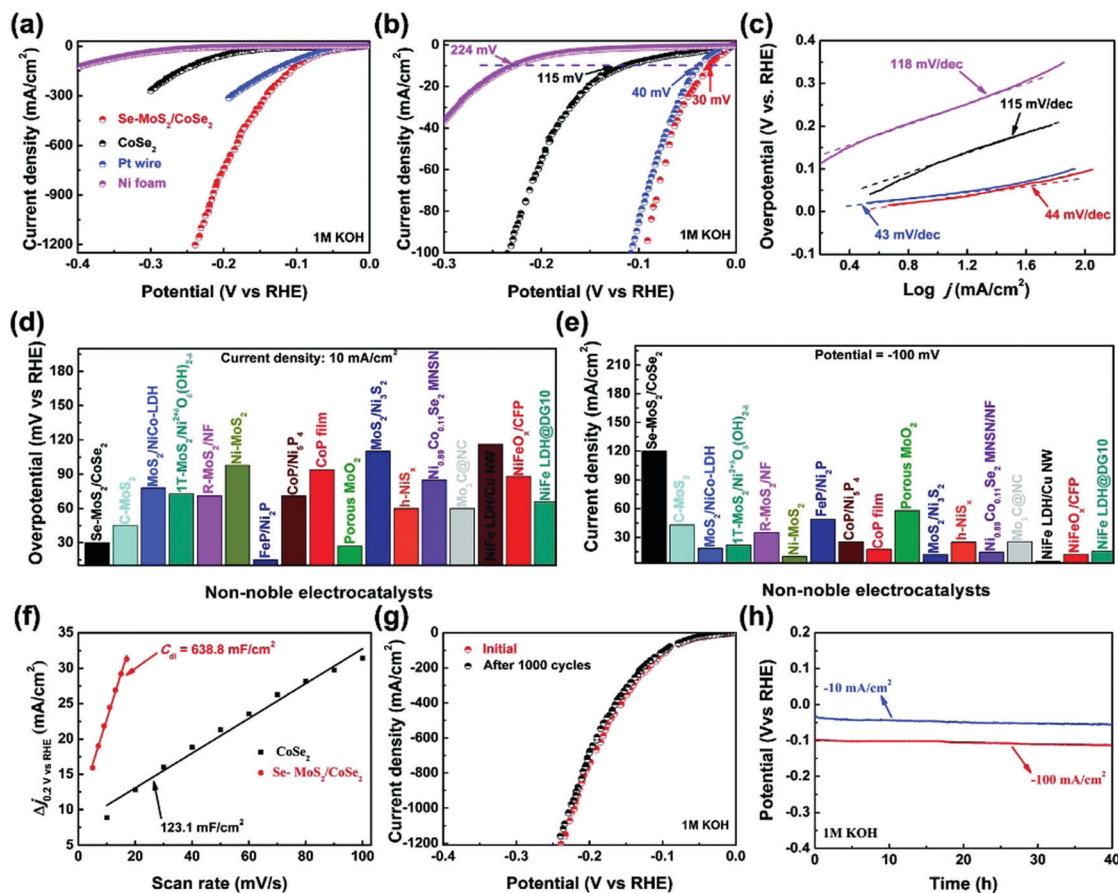
Fig. 9 Electrochemical performance of the Se-MoS$_2$/CoSe$_2$ hybrid catalyst in base. (a and b) The polarization curves of the as-prepared Se-MoS$_2$/CoSe$_2$ hybrid catalyst in comparison with the CoSe$_2$ support, Ni foam, and a Pt wire. (c) Tafel plots of the relevant catalysts in panel (a). Comparison of the investigated hybrid catalyst with other reported ones thus far. (d) Overpotentials at 10 mA cm^{-2}; (e) current densities at −100 mV. (f) The extracted double-layer capacitances (C_{dl}) of the Se-MoS$_2$/CoSe$_2$ hybrid and CoSe$_2$ support. (g) Cyclic stability and (h) time-dependent potential response of the Se-MoS$_2$/CoSe$_2$ hybrid.[83] Reproduced with permission from ref. 83. Copyright 2020, Wiley-VCH.

700 °C, requiring 262 mV at 10 mA cm^{-2} (Fig. 11a–c).[92] Similarly, the FeNi foam surface formed a loosely porous structure composed of numerous nanoparticles, requiring 272 mV at 10 mA cm^{-2}.[93] These nanostructures of transition metal borides exhibited the coupling of crystalline and amorphous structure, conducive to expose more active sites. Also, benefiting from the bimetallic component, the electronic structure can be effectively regulated to reduce adsorption energy.

Transition metal phosphides, sulfides, selenides, tellurides, etc. also had been widely investigated as electrocatalysts for oxygen evolution via solid–vapor treatment, and the rational design of catalysts is also an important concern.[94–96] Hollow and conductive Fe–Co–P alloys as excellent OER electrocatalysts were developed by carbonization and phosphidation of the Fe–Co metal–organic complex (MOC).[97] The structure of the Fe–Co MOC consists of highly uniform nanospheres. The formation of these nanospheres was associated with the Ostwald ripening process. Based on XANES and EXAFS results, high-valent state FeOOH was generated on the surface as the major oxidized species, while most of the Co component retained its low-valent nature during the OER process. The electrochemically induced high valent Fe can stabilize the low valent Co, enabling

enhancement of both OER activity and stability. The multi-functional alloy OER catalyst had an overpotential as low as 252 mV at 10 mA cm^{-2}. Similarly, Qiu et al.[98] firstly performed density functional theory (DFT) calculations to investigate the effect of P doping on the electronic structure of Co$_9$S$_8$ (Fig. 12). Upon the incorporation of phosphorus into lattice sulfur atoms in Co$_9$S$_8$, the calculated density of states (DOS) of P-Co$_9$S$_8$ exhibited an obvious increased electron density at the Fermi level, indicating that P atoms play a vital role in improving the electrical conductivity of Co$_9$S$_8$. Then they constructed P doped Co$_9$S$_8$ nanocages as water oxidation catalysts via hard templates and phosphorization annealing strategy. The P-Co$_9$S$_8$ nanocages allow highly efficient oxygen evolution catalysis, achieving a low overpotential of 280 mV at 10 mA cm^{-2} and long catalytic durability. A 3D bimetallic telluride (CoNiTe$_2$/NF) consisting of a carnation-like structure was synthesized by a hydrothermal and calcination method.[99] Benefitting by the incorporation of the bimetallic telluride and the 3D structure, it shows significant OER activity, which needs overpotentials of $\eta_{10} = 181$ mV, $\eta_{500} = 230$ mV and $\eta_{1000} = 270$ mV. Furthermore, it also exhibits good stability after holding the current density at 100, 500 and 1000 mA cm^{-2} for 24 h, respectively.
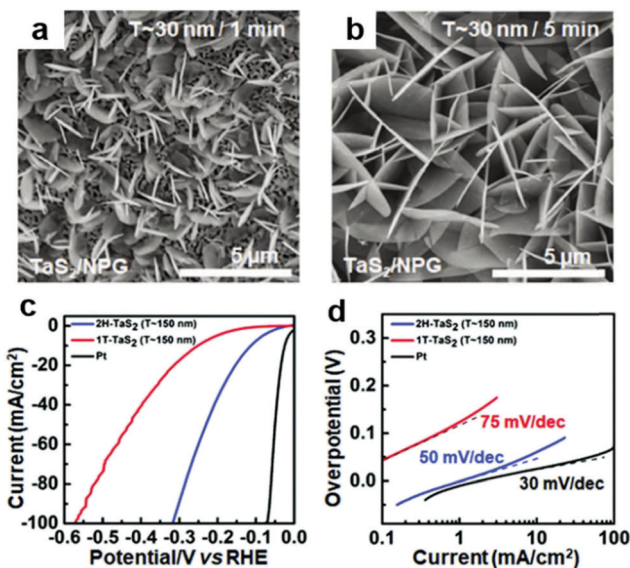
Fig. 10 (a and b) SEM images of 1T-TaS$_2$ with different thicknesses and domain sizes ($T \approx 30$ nm/1 min and $T \approx 30$ nm/5 min, respectively). (c) Polarization curves of 2H-TaS$_2$ on Au foils, 1T-TaS$_2$ on Au foils, and commercial Pt, respectively. (d) Corresponding Tafel plots of the different samples in panel (c).[89] Reproduced with permission from ref. 89. Copyright 2018, Wiley-VCH.
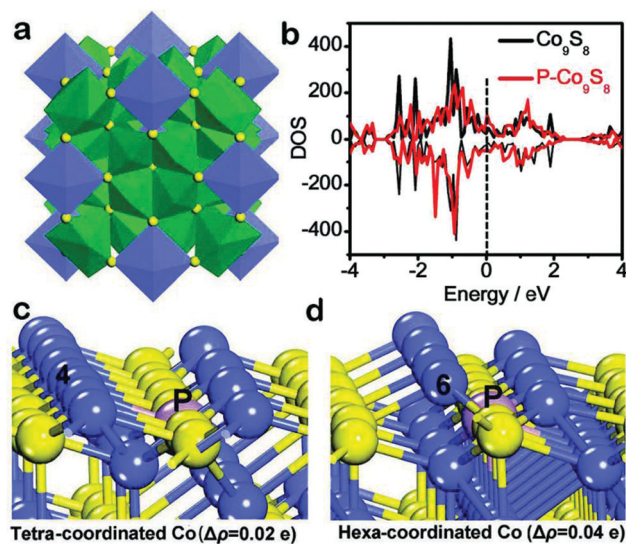

Fig. 12 (a) Structure of Co$_9$S$_8$. The CoS$_6$ coordination octahedra (blue) and CoS$_4$ coordination tetrahedra (green) are shown. (b) The calculated density of states (DOS) of Co$_9$S$_8$ and P-Co$_9$S$_8$, and the black dotted line marks the increased DOS at the Fermi level after P doping. The Bader charge change on (c) tetra-coordinated and (d) hexa-coordinated Co atoms caused by P incorporation, $\Delta\rho$ is the Bader charge change and positive values mean the increment of the outmost electrons as compared to pristine Co$_9$S$_8$.[98] Reproduced with permission from ref. 98. Copyright 2019, Wiley-VCH.

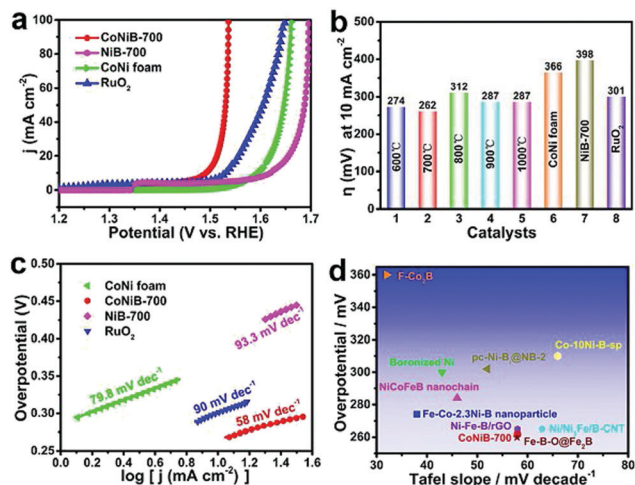**Fig. 11** (a) Polarization curves of CoNi foam, CoNiB-700, NiB-700, and RuO$_2$ toward the OER. (b) Bar graph of the overpotentials at 10 mA cm^{-2} of CoNi foam, CoNiB-600–1000, NiB-700, and RuO$_2$. (c) Tafel slopes. (d) Comparison of the overpotentials and Tafel slopes of CoNiB-700 with other transition metal borides in 1.0 M KOH at 10 mA cm^{-2}.[92] Reproduced with permission from ref. 92. Copyright 2020, Wiley-VCH.

Overall water splitting

To date, numerous potential earth-abundant material candidates have been designed for HER and OER. Unfortunately, HER and OER electrocatalytic candidates generally perform well in different media. The incompatible integration of HER and OER electrocatalysts in the same electrolyte often results in inferior performance of overall water electrolysis. To date,

overall acidic water splitting suffers from the use of scarce and expensive acid-insoluble OER electrocatalysts with passable activity. Overall alkaline water splitting as a promising candidate for commercialization toward mass hydrogen production bears the low activity of HER electrocatalysts under strong alkaline conditions.[100–102] As such, it is attractive to fabricate a bifunctional catalyst that simultaneously exhibits high activity for both HER and OER at pH 0–14, in order to improve the overall water-splitting efficiency, simplify the system, and speed up the commercialization of water splitting.[103] Recently, the controllable integration of HER and OER catalysts into one nanocomposite with the expected synergetic electrocatalysis for both HER and OER has become one of the hottest research topics in the field.[104,105] Among these, solid–vapor methodology is an effective strategy to develop self-supported porous electrodes.[106,107] For instance, Zhao *et al.*[108] report a controllable synthesis strategy for nickel–cobalt bimetal phosphide nanotubes as efficient electrocatalysts for overall water splitting *via* low-temperature phosphorization from a bimetallic metal–organic framework precursor. By optimizing the molar ratio of Co/Ni atoms in MOF-74, a series of Co$_x$Ni$_y$P catalysts were synthesized.[109,110] Benefiting from the unique advantage of MOF-74, which can coordinate with different metal centers without affecting the underlying framework structure, the obtained Co$_4$Ni$_1$P nanotubes possess similar morphology to their MOF precursor and exhibit perfect dispersal of the active sites. The electrolyzer with Co$_4$Ni$_1$P nanotubes as both cathode and anode catalysts in alkaline solutions achieved a current density of 10 mA cm^{-2} at a voltage of 1.59 V, which is even better than that of the
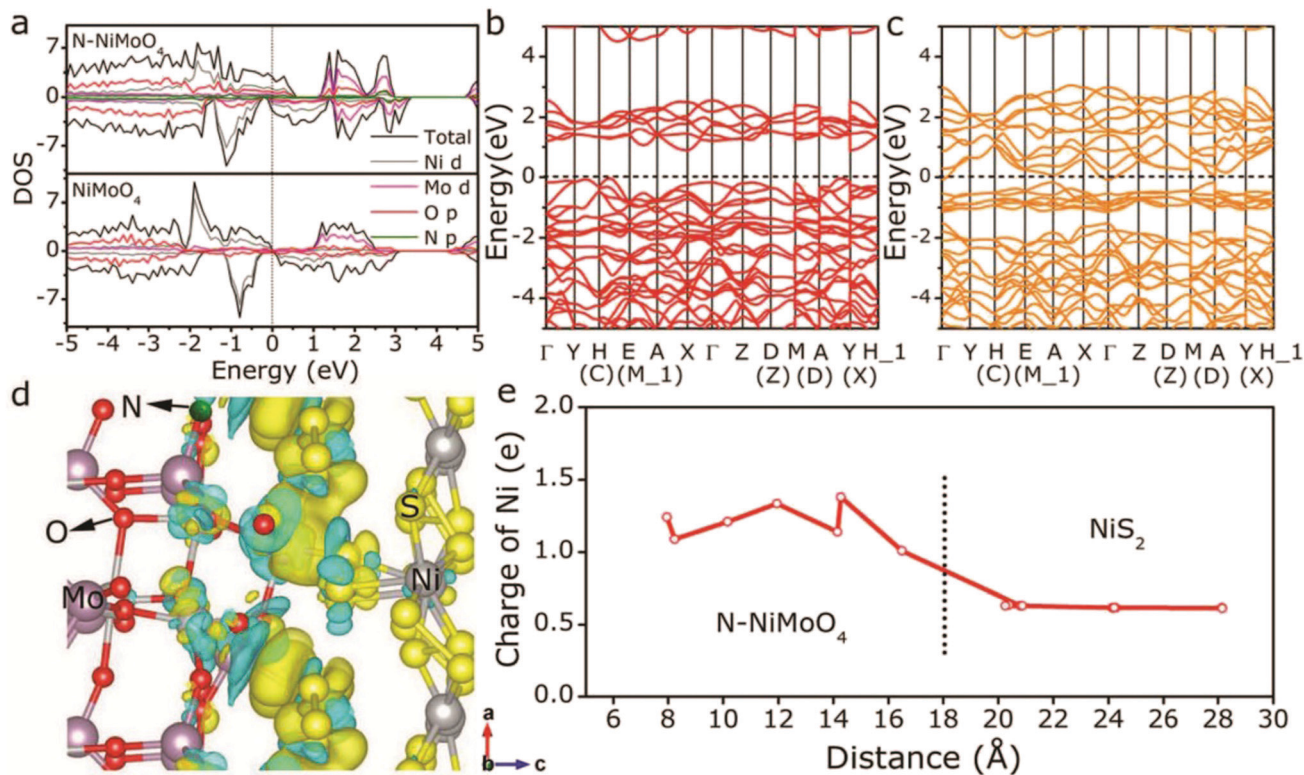
Fig. 13 (a) Projected density of states of N–NiMoO$_4$ and NiMoO$_4$. (b) Band structure of pristine NiMoO$_4$. (c) Band structure of N–NiMoO$_4$. (d) Differential charge density of the N–NiMoO$_4$/NiS$_2$ heterojunction. The increase and decrease of electron density is indicated by the yellow delocalized section and blue delocalized section, respectively. (e) Bader charge analysis of Ni cations along the direction of N–NiMoO$_4$ → NiS$_2$ via the epitaxial heterogeneous interface.[114] Reproduced with permission from ref. 114. Copyright 2018, Wiley-VCH.

integrated Pt/C and RuO$_2$ counterparts. The high performance may be attributed to the large active surface area and the porosity of Co$_4$Ni$_1$P nanotubes, the high conductivity of carbon, and the synergistic effect of NiCoP and Co$_2$P encapsulated within the nanotube morphology. Wang *et al.* synthesized an electrocatalyst of cobalt telluride nanoparticles encapsulated in nitrogen-doped carbon nanotube frameworks (CoTe$_2$@NCNTFs) by a straightforward telluride process under a hydrogen atmosphere using ZIF-67 as the template for overall water splitting. And the CoTe$_2$@NCNTF couple electrolyzer could obtain a current density of 10 mA cm^{-2} at a potential of 1.67 V.[111]

The performance of efficient electrocatalysts largely depends on their geometric morphology, active defects, and electronic regulation.[112,113] For example, a novel kind of N–NiMoO$_4$/NiS$_2$ nanowire/nanosheet has been successfully fabricated with controllable nitridation to activate Ni sites and subsequent vulcanization to induce abundant epitaxial heterogeneous interfaces.[114] Due to differential charge density of the N–NiMoO$_4$/NiS$_2$ heterojunction, electrons transferred from N–NiMoO$_4$ to NiS$_2$, which can stabilize the H adatom and thus benefit the HER performance (Fig. 13). In contrast, the resulting decreased valence state of Ni in N–NiMoO$_4$ would be more efficient for the OER. The bifunctional N–NiMoO$_4$/NiS$_2$ electrodes delivered a current density of 10 mA cm^{-2} at a cell voltage of 1.60 V, 3.39 times higher than that of the Pt–Ir system (2.95 mA cm^{-2}), and maintained 10 h long-term stability at 10 mA cm^{-2}.

Conclusion and perspective

In summary, advances in electrochemical catalysts fabricated by solid–vapor methodology have been evaluated and summarized. It was found that solid–vapor treatment demonstrates versatile applications in hierarchical nanostructure engineering and exhibits great potential in electrode development. Firstly, the procedure and mechanism of the fabrication process have been investigated. Specifically, we have summarized various morphologies developed for the efficient catalysts with respect to a large surface area and porous structure, including nanoparticles, nanowires, nanorods, nanosheets, *etc.* Subsequently, an overview of the application of the as-prepared electrodes is provided mainly focused on electrochemical water splitting (HER, OER and overall water splitting).

Despite great efforts invested in transition metal-based hierarchical porous catalysts for water splitting, there are still a number of aspects in this field that need to be improved. (1) Although the solid–vapor methods could synthesize numerous materials with different components and structures, there is still little known about the nature of the intermediates and impurities during the synthetic procedure. Thus, how to select the reaction raw materials and precursors to induce the configuration of high-quality catalysts with understanding at the molecular/atomic level and controllable large-scale engineering optimization for commercial applications is yet

an unresolved challenge. (2) The performance improvement of most of the multi-compositional catalysts reported in the literature is attributed to the synergistic effects between the different components without authentic understanding, which greatly restricts the optimization and integration of heterogeneous catalysts. Utilization of *in situ* characterization techniques, such as *in situ* TEM, XAS, and FTIR, can offer indeed valuable evidence for unveiling the intermolecular interaction even within time-resolution and spatial resolution measurement. (3) With the development of synthetic strategies and in-depth understanding of the relation among the structure, catalytic performance and mechanism, the development of novel catalysts with facile configuration, low cost and excellent catalytic properties is in great demand.

Conflicts of interest

There are no conflicts to declare.

Acknowledgements

Notes and references

1 F. Lyu, Q. Wang, S. M. Choi and Y. Yin, *Small*, 2019, **15**, 1804201.
2 B. Xiong, L. Chen and J. Shi, *ACS Catal.*, 2018, **8**, 3688–3707.
3 X. Zou and Y. Zhang, *Chem. Soc. Rev.*, 2015, **44**, 5148–5180.
4 Y. Wang, B. Kong, D. Zhao, H. Wang and C. Selomulya, *Nano Today*, 2017, **15**, 26–55.
5 Y. Shi and B. Zhang, *Chem. Soc. Rev.*, 2016, **45**, 1529–1541.
6 Q. Lu, Y. Yu, Q. Ma, B. Chen and H. Zhang, *Adv. Mater.*, 2016, **28**, 1917–1933.
7 C. G. Morales-Guio, L. A. Stern and X. Hu, *Chem. Soc. Rev.*, 2014, **43**, 6555–6569.
8 S. Anantharaj, S. R. Ede, K. Sakthikumar, K. Karthick, S. Mishra and S. Kundu, *ACS Catal.*, 2016, **6**, 8069–8097.
9 X. Li, X. Hao, A. Abudula and G. Guan, *J. Mater. Chem. A*, 2016, **4**, 11973–12000.
10 S. Sultan, J. N. Tiwari, A. N. Singh, S. Zhumagali, M. Ha, C. W. Myung, P. Thangavel and K. S. Kim, *Adv. Energy Mater.*, 2019, **9**, 1900624.
11 D. Zhou, P. Li, W. Xu, S. Jawaid, J. Mohammed-Ibrahim, W. Liu, Y. Kuang and X. Sun, *ChemNanoMat*, 2020, **6**, 336–355.
12 A.-M. Alexander and J. S. J. Hargreaves, *Chem. Soc. Rev.*, 2010, **39**, 4388–4401.

13 D. Wang, Y. Song, H. Zhang, X. Yan and J. Guo, *J. Electroanal. Chem.*, 2020, **861**, 113953.
14 Y. Guo, T. Park, J. W. Yi, J. Henzie, J. Kim, Z. Wang, B. Jiang, Y. Bando, Y. Sugahara, J. Tang and Y. Yamauchi, *Adv. Mater.*, 2019, **31**, e1807134.
15 H. Sun, Z. Yan, F. Liu, W. Xu, F. Cheng and J. Chen, *Adv. Mater.*, 2020, **32**, e1806326.
16 L. Zeng, K. Sun, X. Wang, Y. Liu, Y. Pan, Z. Liu, D. Cao, Y. Song, S. Liu and C. Liu, *Nano Energy*, 2018, **51**, 26–36.
17 Y. Zhang, L. Zhang and C. Zhou, *Acc. Chem. Res.*, 2013, **46**, 2329–2339.
18 C. R. Zhu, D. Gao, J. Ding, D. Chao and J. Wang, *Chem. Soc. Rev.*, 2018, **47**, 4332–4356.
19 M. Sun, H. Liu, J. Qu and J. Li, *Adv. Energy Mater.*, 2016, **6**, 1600087.
20 T. Liu, X. Ma, D. Liu, S. Hao, G. Du, Y. Ma, A. M. Asiri, X. Sun and L. Chen, *ACS Catal.*, 2017, **7**, 98–102.
21 C. Wu, Y. Yang, D. Dong, Y. Zhang and J. Li, *Small*, 2017, **13**, 1602873.
22 K. Liang, S. Pakhira, Z. Yang, A. Nijamudheen, L. Ju, M. Wang, C. I. Aguirre-Velez, G. E. Sterbinsky, Y. Du, Z. Feng, J. L. Mendoza-Cortes and Y. Yang, *ACS Catal.*, 2019, **9**, 651–659.
23 X. Wang, Z. Ma, L. Chai, L. Xu, Z. Zhu, Y. Hu, J. Qian and S. Huang, *Carbon*, 2019, **141**, 643–651.
24 X. Zhang, X. Yu, L. Zhang, F. Zhou, Y. Liang and R. Wang, *Adv. Funct. Mater.*, 2018, **28**, 1706523.
25 J. Yang, F. Zhang, X. Wang, D. He, G. Wu, Q. Yang, X. Hong, Y. Wu and Y. Li, *Angew. Chem., Int. Ed.*, 2016, **55**, 12854–12858.
26 H. Zhou, F. Yu, J. Sun, H. Zhu, I. K. Mishra, S. Chen and Z. Ren, *Nano Lett.*, 2016, **16**, 7604–7609.
27 Q. Li, N. Li, J. An and H. Pang, *Inorg. Chem. Front.*, 2020, **7**, 2089–2096.
28 X. Xiao, C.-T. He, S. Zhao, J. Li, W. Lin, Z. Yuan, Q. Zhang, S. Wang, L. Dai and D. Yu, *Energy Environ. Sci.*, 2017, **10**, 893–899.
29 J. Zhuo, M. Caban-Acevedo, H. Liang, L. Samad, Q. Ding, Y. Fu, M. Li and S. Jin, *ACS Catal.*, 2015, **5**, 6355–6361.
30 Z. Wu, B. Fang, A. Bonakdarpour, A. Sun, D. P. Wilkinson and D. Wang, *Appl. Catal., B*, 2012, **125**, 59–66.
31 C. Xu, Q. Li, J. Shen, Z. Yuan, J. Ning, Y. Zhong, Z. Zhang and Y. Hu, *Nanoscale*, 2019, **11**, 10738–10745.
32 H. Zhou, F. Yu, Y. Huang, J. Sun, Z. Zhu, R. J. Nielsen, R. He, J. Bao, W. A. Goddard, III, S. Chen and Z. Ren, *Nat. Commun.*, 2016, **7**, 12765.
33 S. Jing, L. Zhang, L. Luo, J. Lu, S. Yin, P. K. Shen and P. Tsiakaras, *Appl. Catal., B*, 2018, **224**, 533–540.
34 X. Ji, R. Zhang, X. Shi, A. M. Asiri, B. Zheng and X. Sun, *Nanoscale*, 2018, **10**, 7941–7945.
35 Z. Ali, M. Asif, T. Zhang, X. Huang and Y. Hou, *Small*, 2019, **15**, e1901995.
36 K. Deng, T. Ren, Y. Xu, S. Liu, Z. Dai, Z. Wang, X. Li, L. Wang and H. Wang, *J. Mater. Chem. A*, 2020, **8**, 5595–5600.
37 Y. Huan, J. Shi, X. Zou, Y. Gong, C. Xie, Z. Yang, Z. Zhang, Y. Gao, Y. Shi, M. Li, P. Yang, S. Jiang, M. Hong, L. Gu,

Q. Zhang, X. Yan and Y. Zhang, *J. Am. Chem. Soc.*, 2019, **141**, 18694–18703.

38 C.-P. Lee, W.-F. Chen, T. Billo, Y.-G. Lin, F.-Y. Fu, S. Samireddi, C.-H. Lee, J.-S. Hwang, K.-H. Chen and L.-C. Chen, *J. Mater. Chem. A*, 2016, **4**, 4553–4561.

39 I. K. Mishra, H. Zhou, J. Sun, F. Qin, K. Dahal, J. Bao, S. Chen and Z. Ren, *Energy Environ. Sci.*, 2018, **11**, 2246–2252.

40 R. Zhang, X. Wang, S. Yu, T. Wen, X. Zhu, F. Yang, X. Sun, X. Wang and W. Hu, *Adv. Mater.*, 2017, **29**, 1605502.

41 C. Guan, W. Xiao, H. Wu, X. Liu, W. Zang, H. Zhang, J. Ding, Y. P. Feng, S. J. Pennycook and J. Wang, *Nano Energy*, 2018, **48**, 73–80.

42 X. Xiao, L. Tao, M. Li, X. Lv, D. Huang, X. Jiang, H. Pan, M. Wang and Y. Shen, *Chem. Sci.*, 2018, **9**, 1970–1975.

43 P. Xiao, W. Chen and X. Wang, *Adv. Energy Mater.*, 2015, **5**, 1500985.

44 H. Wu, X. Lu, G. Zheng and G. W. Ho, *Adv. Energy Mater.*, 2018, **8**, 1702704.

45 D. Y. Chung, S. W. Jun, G. Yoon, H. Kim, J. M. Yoo, K.-S. Lee, T. Kim, H. Shin, A. K. Sinha, S. G. Kwon, K. Kang, T. Hyeon and Y.-E. Sung, *J. Am. Chem. Soc.*, 2017, **139**, 6669–6674.

46 F.-S. Zhang, J.-W. Wang, J. Luo, R.-R. Liu, Z.-M. Zhang, C.-T. He and T.-B. Lu, *Chem. Sci.*, 2018, **9**, 1375–1384.

47 R. Ye, P. del Angel-Vicente, Y. Liu, M. J. Arellano-Jimenez, Z. Peng, T. Wang, Y. Li, B. I. Yakobson, S.-H. Wei, M. J. Yacaman and J. M. Tour, *Adv. Mater.*, 2016, **28**, 1427–1432.

48 Y. Zuo, D. Rao, S. Ma, T. Li, Y. H. Tsang, S. Kment and Y. Chai, *ACS Nano*, 2019, **13**, 11469–11476.

49 J. Yu, W.-J. Li, H. Zhang, F. Zhou, R. Li, C.-Y. Xu, L. Zhou, H. Zhong and J. Wang, *Nano Energy*, 2019, **57**, 222–229.

50 F. Yu, H. Zhou, Y. Huang, J. Sun, F. Qin, J. Bao, W. A. Goddardiii, S. Chen and Z. Ren, *Nat. Commun.*, 2018, **9**, 2551.

51 P. Jiang, Q. Liu, Y. Liang, J. Tian, A. M. Asiri and X. Sun, *Angew. Chem., Int. Ed.*, 2014, **53**, 12855–12859.

52 J. Tian, Q. Liu, A. M. Asiri and X. Sun, *J. Am. Chem. Soc.*, 2014, **136**, 7587–7590.

53 R. Zhang, C. Tang, R. Kong, G. Du, A. M. Asiri, L. Chen and X. Sun, *Nanoscale*, 2017, **9**, 4793–4800.

54 J. Tian, Q. Liu, N. Cheng, A. M. Asiri and X. Sun, *Angew. Chem., Int. Ed.*, 2014, **53**, 9577–9581.

55 J.-X. Feng, S.-Y. Tong, Y.-X. Tong and G.-R. Li, *J. Am. Chem. Soc.*, 2018, **140**, 5118–5126.

56 N. Yao, P. Li, Z. Zhou, R. Meng, G. Cheng and W. Luo, *Small*, 2019, **15**, e1901993.

57 P. Kuang, T. Tong, K. Fan and J. Yu, *ACS Catal.*, 2017, **7**, 6179–6187.

58 M. Wang, W. J. Zhang, F. F. Zhang, Z. H. Zhang, B. Tang, J. P. Li and X. G. Wang, *ACS Catal.*, 2019, **9**, 1489–1502.

59 L. Yang, L. Loh, D. K. Nandakumar, W. Lu, M. Gao, X. L. C. Wee, K. Zeng, M. Bosman and S. C. Tan, *Adv. Mater.*, 2020, **32**, e2000971.

60 J. Yin, J. Jin, H. Zhang, M. Lu, Y. Peng, B. Huang, P. Xi and C. H. Yan, *Angew. Chem., Int. Ed.*, 2019, **58**, 18676–18682.

61 B. Zhang, Y. H. Lui, H. Ni and S. Hu, *Nano Energy*, 2017, **38**, 553–560.

62 X. Hu, S. Zhang, J. Sun, L. Yu, X. Qian, R. Hu, Y. Wang, H. Zhao and J. Zhu, *Nano Energy*, 2019, **56**, 109–117.

63 X. Wang, Y. V. Kolen'ko, X. Q. Bao, K. Kovnir and L. Liu, *Angew. Chem., Int. Ed.*, 2015, **54**, 8188–8192.

64 X. Wang, W. Li, D. Xiong, D. Y. Petrovykh and L. Liu, *Adv. Funct. Mater.*, 2016, **26**, 4067–4077.

65 X. Wang, W. Li, D. Xiong and L. Liu, *J. Mater. Chem. A*, 2016, **4**, 5639–5646.

66 Z. Ma, R. Li, M. Wang, H. Meng, F. Zhang, X.-Q. Bao, B. Tang and X. Wang, *Electrochim. Acta*, 2016, **219**, 194–203.

67 R. Boppella, J. Tan, W. Yang and J. Moon, *Adv. Funct. Mater.*, 2018, **29**, 1807976.

68 Z. Fang, L. Peng, Y. Qian, X. Zhang, Y. Xie, J. J. Cha and G. Yu, *J. Am. Chem. Soc.*, 2018, **140**, 5241–5247.

69 Y. Sun, K. Xu, Z. Wei, H. Li, T. Zhang, X. Li, W. Cai, J. Ma, H. J. Fan and Y. Li, *Adv. Mater.*, 2018, **30**, e1802121.

70 J. Wu, T. Chen, C. Zhu, J. Du, L. Huang, J. Yan, D. Cai, C. Guan and C. Pan, *ACS Sustainable Chem. Eng.*, 2020, **8**, 4474–4480.

71 Y. Lian, H. Sun, X. Wang, P. Qi, Q. Mu, Y. Chen, J. Ye, X. Zhao, Z. Deng and Y. Peng, *Chem. Sci.*, 2019, **10**, 464–474.

72 Y. Pan, K. Sun, Y. Lin, X. Cao, Y. Cheng, S. Liu, L. Zeng, W.-C. Cheong, D. Zhao, K. Wu, Z. Liu, Y. Liu, D. Wang, Q. Peng, C. Chen and Y. Li, *Nano Energy*, 2019, **56**, 411–419.

73 Y. Yang, Y. Kang, H. Zhao, X. Dai, M. Cui, X. Luan, X. Zhang, F. Nie, Z. Ren and W. Song, *Small*, 2020, **16**, e1905083.

74 M. Liu and J. Li, *ACS Appl. Mater. Interfaces*, 2016, **8**, 2158–2165.

75 B. You, N. Jiang, M. Sheng, S. Gul, J. Yano and Y. Sun, *Chem. Mater.*, 2015, **27**, 7636–7642.

76 B. He, X. C. Wang, L. X. Xia, Y. Q. Guo, Y. W. Tang, Y. Zhao, Q. L. Hao, T. Yu, H. K. Liu and Z. Su, *ChemSusChem*, 2020, **13**, 5239.

77 Q. Xu, H. Pang, H. Xue, Q. Li and S. Zheng, *Natl. Sci. Rev.*, 2020, **7**, 305–314.

78 A. Indra, T. Song and U. Paik, *Adv. Mater.*, 2018, **30**, 1705146.

79 Y. Pan, K. Sun, S. Liu, X. Cao, K. Wu, W. C. Cheong, Z. Chen, Y. Wang, Y. Li, Y. Liu, D. Wang, Q. Peng, C. Chen and Y. Li, *J. Am. Chem. Soc.*, 2018, **140**, 2610–2618.

80 H. F. Wang, L. Chen, H. Pang, S. Kaskel and Q. Xu, *Chem. Soc. Rev.*, 2020, **49**, 1414–1448.

81 Z.-H. Xue, H. Su, Q.-Y. Yu, B. Zhang, H.-H. Wang, X.-H. Li and J.-S. Chen, *Adv. Energy Mater.*, 2017, **7**, 1602355.

82 K. Xu, H. Ding, M. Zhang, M. Chen, Z. Hao, L. Zhang, C. Wu and Y. Xie, *Adv. Mater.*, 2017, **29**, 1606980.

83 L. Liao, J. Sun, D. Li, F. Yu, Y. Zhu, Y. Yang, J. Wang, W. Zhou, D. Tang, S. Chen and H. Zhou, *Small*, 2020, **16**, e1906629.

84 J. Sun, M. Ren, L. Yu, Z. Yang, L. Xie, F. Tian, Y. Yu, Z. Ren, S. Chen and H. Zhou, *Small*, 2019, **15**, 1804272.

85 W. Li, S. Zhang, Q. Fan, F. Zhang and S. Xu, *Nanoscale*, 2017, **9**, 5677–5685.

86 H. Zhu, J. Zhang, R. Yanzhang, M. Du, Q. Wang, G. Gao, J. Wu, G. Wu, M. Zhang, B. Liu, J. Yao and X. Zhang, *Adv. Mater.*, 2015, **27**, 4752–4759.

87 H. Liu, X. Qian, Y. Niu, M. Chen, C. Xu and K.-Y. Wong, *Chem. Eng. J.*, 2020, **383**, 123129.

88 L. Najafi, S. Bellani, R. Oropesa-Nuñez, B. Martín-García, M. Prato, L. Pasquale, J.-K. Panda, P. Marvan, Z. Sofer and F. Bonaccorso, *ACS Catal.*, 2020, **10**, 3313–3325.

89 Y. Huan, J. Shi, X. Zou, Y. Gong, Z. Zhang, M. Li, L. Zhao, R. Xu, S. Jiang, X. Zhou, M. Hong, C. Xie, H. Li, X. Lang, Q. Zhang, L. Gu, X. Yan and Y. Zhang, *Adv. Mater.*, 2018, **30**, e1705916.

90 H. Han, H. Choi, S. Mhin, Y.-R. Hong, K. M. Kim, J. Kwon, G. Ali, K. Y. Chung, M. Je, H. N. Umh, D.-H. Lim, K. Davey, S.-Z. Qiao, U. Paik and T. Song, *Energy Environ. Sci.*, 2019, **12**, 2443–2454.

91 W. Li, Y. Niu, X. Wu, F. Wu, T. Li and W. Hu, *ACS Sustainable Chem. Eng.*, 2020, **8**, 4658–4666.

92 H. Yuan, S. Wei, B. Tang, Z. Ma, J. Li, M. Kundu and X. Wang, *ChemSusChem*, 2020, **13**, 3662–3670.

93 H. Yuan, S. Wang, X. Gu, B. Tang, J. Li and X. Wang, *J. Mater. Chem. A*, 2019, **7**, 19554–19564.

94 S. Zhang, Y. Li, H. Zhu, S. Lu, P. Ma, W. Dong, F. Duan, M. Chen and M. Du, *ACS Appl. Mater. Interfaces*, 2020, **12**, 6250–6261.

95 J. Zhang, X. Bai, T. Wang, W. Xiao, P. Xi, J. Wang, D. Gao and J. Wang, *Nano-Micro Lett.*, 2019, **11**, 2.

96 X. Zhang, X. Zhang, H. Xu, Z. Wu, H. Wang and Y. Liang, *Adv. Funct. Mater.*, 2017, **27**, 1606635.

97 K. Liu, C. Zhang, Y. Sun, G. Zhang, X. Shen, F. Zou, H. Zhang, Z. Wu, E. C. Wegener, C. J. Taubert, J. T. Miller, Z. Peng and Y. Zhu, *ACS Nano*, 2018, **12**, 158–167.

98 B. Qiu, L. Cai, Y. Wang, X. Guo, S. Ma, Y. Zhu, Y. H. Tsang, Z. Zheng, R. Zheng and Y. Chai, *Small*, 2019, **15**, e1904507.

99 G. Qian, Y. Mo, C. Yu, H. Zhang, T. Yu, L. Luo and S. Yin, *Renewable Energy*, 2020, **162**, 2190–2196.

100 A. Han, H. Zhang, R. Yuan, H. Ji and P. Du, *ACS Appl. Mater. Interfaces*, 2017, **9**, 2240–2248.

101 L. Fang, W. Li, Y. Guan, Y. Feng, H. Zhang, S. Wang and Y. Wang, *Adv. Funct. Mater.*, 2017, **27**, 1701008.

102 B. You, N. Jiang, M. Sheng, M. W. Bhushan and Y. Sun, *ACS Catal.*, 2016, **6**, 714–721.

103 G.-F. Chen, T. Y. Ma, Z.-Q. Liu, N. Li, Y.-Z. Su, K. Davey and S.-Z. Qiao, *Adv. Funct. Mater.*, 2016, **26**, 3314–3323.

104 C. Du, L. Yang, F. Yang, G. Cheng and W. Luo, *ACS Catal.*, 2017, **7**, 4131–4137.

105 X. Xiao, D. Huang, X. Fu, M. Wen, X. Jiang, X. Lv, M. Li, L. Gao, S. Liu, M. Wang, C. Zhao and Y. Shen, *ACS Appl. Mater. Interfaces*, 2018, **10**, 4689–4696.

106 Y. Li, H. Zhang, M. Jiang, Q. Zhang, P. He and X. Sun, *Adv. Funct. Mater.*, 2017, **27**, 1702513.

107 Y. Wu, F. Li, W. Chen, Q. Xiang, Y. Ma, H. Zhu, P. Tao, C. Song, W. Shang, T. Deng and J. Wu, *Adv. Mater.*, 2018, **30**, e1803151.

108 L. Yan, L. Cao, P. Dai, X. Gu, D. Liu, L. Li, Y. Wang and X. Zhao, *Adv. Funct. Mater.*, 2017, **27**, 1703455.

109 Y. Guo, P. Yuan, J. Zhang, H. Xia, F. Cheng, M. Zhou, J. Li, Y. Qiao, S. Mu and Q. Xu, *Adv. Funct. Mater.*, 2018, **28**, 1805641.

110 W. Li, X. Gao, D. Xiong, F. Xia, J. Liu, W. G. Song, J. Xu, S. M. Thalluri, M. F. Cerqueira, X. Fu and L. Liu, *Chem. Sci.*, 2017, **8**, 2952–2958.

111 X. Wang, X. Huang, W. Gao, Y. Tang, P. Jiang, K. Lan, R. Yang, B. Wang and R. Li, *J. Mater. Chem. A*, 2018, **6**, 3684–3691.

112 X. Yao, L. Zhuang, Y. Jia, H. Liu, Z. Li, L. Zhang, X. Wang, D. Yang and Z. Zhu, *Angew. Chem., Int. Ed.*, 2020, **59**, 14664–14670.

113 Z. Liu, C. Zhang, H. Liu and L. Feng, *Appl. Catal., B*, 2020, **276**, 119165.

114 L. An, J. Feng, Y. Zhang, R. Wang, H. Liu, G.-C. Wang, F. Cheng and P. Xi, *Adv. Funct. Mater.*, 2018, **29**, 1805298.